PHYSICAL REVIEW D **89,** 034508 (2014)

Magnetic properties of the nucleon in a uniform background field

Thomas Primer,* Waseem Kamleh, and Derek Leinweber
Special Research Centre for the Subatomic Structure of Matter, School of Chemistry and Physics, University of Adelaide, South Australia 5005, Australia

Matthias Burkardt
Department of Physics, New Mexico State University, Las Cruces, New Mexico 88003-8001, USA
(Received 7 July 2013; published 28 February 2014)

We present results for the magnetic moment and magnetic polarizability of the neutron and the magnetic moment of the proton. These results are calculated using the uniform background field method on $32^3 \times 64$ dynamical QCD lattices provided by the PACS-CS Collaboration as part of the ILDG. We use a uniform background magnetic field quantized by the periodic spatial volume. We investigate ways to improve the effective energy plots used to calculate magnetic polarizabilities, including the use of correlation matrix techniques with various source smearings.

DOI: 10.1103/PhysRevD.89.034508 PACS numbers: 12.38.Gc, 13.40.-f, 13.40.Em

I. INTRODUCTION

The magnetic moment and magnetic polarizability are fundamental properties of a particle that describe its response to an external magnetic field. Developing the ability to calculate these properties via the first principles approach of lattice QCD is important. There are two well-known techniques for calculating magnetic moments on the lattice. One is the three-point function method [1–3], which is used to calculate baryon electromagnetic form factors that can be converted into magnetic moments by performing an extrapolation to zero momentum. The other is the background field method [4–14], which uses a phase factor on the gauge links to induce an external field across the whole lattice. This external field causes an energy shift from which the magnetic moment and polarizability can be derived by making use of the following energy-field relation [4,15]:

$$E(B) = M_N - \vec{\mu}\cdot\vec{B} + \frac{e|B|}{2M_N} - \frac{4\pi}{2}\beta B^2 + \mathcal{O}(B^3), \qquad (1)$$

defining $\vec{\mu}$ as the magnetic moment and β as the magnetic polarizability. We note the term $e|B|/2M_N$ is the ground-state Landau energy. In principle, there is a tower of energy levels with energy $(2n+1)e|B|/2M_N$ for $n = 0, 1, 2, \ldots$.

When deriving the background field method on a periodic lattice, there arises a quantization condition which limits the available choices of magnetic field strength based on the size of the lattice [5,6]. If the lattice is too small, the field will be large and higher-order terms in the energy relation of Eq. (1) will begin to dominate [8]. Previous calculations have avoided this problem by using a Dirichlet boundary condition in a spatial dimension and a linearized form of the phase factor, which allows for an arbitrary choice of field strength [12]. We note the linearized form of the link breaks gauge invariance. Others have used the exponential phase, but instead of correcting the value of the field at the boundary, they put the quark origin at the center of the lattice and hope that the boundary is far enough away for the effects of the discontinuity to be small [7]. Using either of these methods introduces finite volume errors which can be hard to predict. A calculation using the periodic boundary conditions and quantized exponential phase factor to create a uniform magnetic field everywhere was done for the delta and omega baryons in Ref. [13]. Our calculation is the first to apply the complete methodology to the nucleon. We present results for both the magnetic moment and the magnetic polarizability of the neutron. For the proton, we present only magnetic moment results, because the Landau levels interfere with polarizability calculations for charged particles.

II. BACKGROUND FIELD METHOD

We make use of the background field method to simulate a constant magnetic field along one axis [6]. The technique is formulated on the lattice by first considering the continuum case, where the covariant derivative is modified by the addition of a minimal electromagnetic coupling,

$$D_\mu = \partial_\mu + igG_\mu + iqA_\mu, \qquad (2)$$

where A_μ is the electromagnetic four-potential and q is the charge on the fermion field. On the lattice, this is equivalent to multiplying the usual gauge links by a simple phase factor

$$U_\mu^{(B)}(x) = \exp(iaqA_\mu(x)). \qquad (3)$$

To obtain a uniform magnetic field along the z axis, we note that $\vec{B} = \vec{\nabla}\times\vec{A}$, and hence

*thomas.primer@adelaide.edu.au

$$B_z = \partial_x A_y - \partial_y A_x. \tag{4}$$

Note that this equation does not specify the gauge potential uniquely; there are multiple valid choices of A_μ that give rise to the same field. We choose $A_x = -By$ to produce a constant magnetic field of magnitude B in the z direction. The resulting field can be checked by examining a single plaquette in the $(\mu, \nu) = (x, y)$ plane, which is related to the magnetic field through the field strength tensor,

$$\square_{\mu\nu}(x) = \exp\left(iqa^2 F_{\mu\nu}(x)\right), \tag{5}$$

which is exact for a constant background field because all higher-order terms involve a second- or higher-order derivative. For a general plaquette at coordinates x, y, the result is

$$\exp(-iaqBy)\exp(iaqB(y+a)) = \exp(ia^2 qB), \tag{6}$$

giving the desired field over most of the lattice. However, on a finite lattice $(0 \le x/a \le N_x - 1)$, $(0 \le y/a \le N_y - 1)$, there is a discontinuity at the boundary due to the periodic boundary conditions. In order to fix this problem we make use of the $\partial_x A_y$ term from Eq. (4), giving A_y the following values:

$$A_y(x, y) = \begin{cases} 0, & \text{for } y/a < N_y - 1 \\ N_y Bx, & \text{for } y/a = N_y - 1 \end{cases}. \tag{7}$$

This ensures that we now get the required value at the $y/a = N_y - 1$ boundary.

There is then the issue of the double boundary, $x/a = N_x - 1$ and $y/a = N_y - 1$, where the plaquette only has the required value under the condition $\exp(-ia^2 qBN_x N_y) = 1$. This gives rise to the quantization condition, which limits the choices of magnetic field strength based on the lattice size:

$$qBa^2 = \frac{2\pi n}{N_x N_y}, \tag{8}$$

where n is an integer specifying the field strength in multiples of the minimum field-strength quantum.

Having specified the $U(1)$ gauge, we note that in addition to a uniform magnetic field, the selected links produce two nontrivial holonomies:

$$H_x(y) = \prod_x U_x(x, y) = e^{-iaN_x qBy}, \tag{9}$$

$$H_y(x) = \prod_y U_y(x, y) = e^{+iaN_y qBx}. \tag{10}$$

The holonomies $H_x(y)$ and $H_y(x)$ are absent for $qBa^2 = 2\pi/N_x$ and $qBa^2 = 2\pi/N_y$, respectively. We note these fields are of order N_x or N_y times the field strengths considered herein and would render the calculation untenable. Analogous to the Polyakov loop, these quantities are gauge invariant and spatially dependent. The possible effects of these holonomies may need to be considered, for example, when attempting to project hadronic correlation functions. Indeed, the use of the lowest (continuum) Landau wave function, including the effects of the holonomies due to the periodic lattice, was studied elsewhere and shown to be effective in the context of scalar field theory [16]. In the present work, our hadronic correlation functions use the standard Fourier-based momentum projection, and as such, we do not include the effects of the holonomies.

III. SIMULATION DETAILS

These calculations use the $2+1$ flavor dynamical-fermion configurations provided by the PACS-CS group [17] through the ILDG [18]. These are $32^3 \times 64$ lattices using a clover fermion action and Iwasaki gauge action with $\beta = 1.9$ and physical lattice spacing $a = 0.0907(13)$ fm. We use four values of the light quark hopping parameter, $\kappa_{ud} = 0.13700, 0.13727, 0.13754, 0.13770$, corresponding to the pion masses $m_\pi = 702, 572, 413, 293$ MeV. The lattice spacing for each mass was set using the Sommer scale with $r_0 = 0.49$ fm. The size of the ensemble was 320 for the two lighter masses and 400 for the heavier ones. Values for $m_\pi L$ range from 10.3 to 4.3.

In order to get correlation functions at four different magnetic field strengths, we calculated propagators at six nonzero field strengths: $qBa^2 = +0.0061, -0.0123, +0.0184, +0.0245, -0.0368, -0.0492$. These correspond to $n = +1, -2, +3, +4, -6$, and -8 in Eq. (8). Using the relationships $q_d = -e/3$ and $q_u = 2e/3$ to combine up and down quark propagators with the appropriate field strengths resulted in hadrons in fields of strength $eB = -0.087, +0.174, -0.261, -0.345$ GeV^2 at the physical lattice spacing. Unless specified otherwise, we used the interpolating field $\chi_1 = (u^T C\gamma_5 d)u$ with 100 sweeps of Gaussian smearing at the source. We put the origin of the electromagnetic gauge field at the same lattice site as the quark origin to ensure that the smeared source maintains good overlap with the ground states.

It should be noted that the configurations are dynamical only in the QCD sense; there was no magnetic field included when they were generated. The background field can be put on the sea quarks by performing a separate HMC calculation for each field strength, but this is obviously very computationally expensive. It also destroys the correlations between the different field strengths, which would lead to much larger errors in the energy shifts used to calculate moments and polarizabilities. While techniques for a reweighting of configurations in order to correct for the background field are under exploration [19], these have not been employed in this work.

Because the light u, d and s quark charges sum to zero, the corrections to the magnetic moment from sea-quark loops is proportional to $SU(3)$ flavor symmetry breaking [20,21]. Through the use of standard three-point function calculations of the magnetic form factors, these contributions are well understood [22–24] and provide a small correction to the neutron moment. However, their direct calculation in the background field formalism remains an interesting challenge.

The contributions of sea-quark loops to the magnetic polarizability are more subtle, due to the consideration of two photon couplings to the quark flow of meson dressings [25,26]. For example, the leading nonanalytic behavior receives sea-quark loop contributions from both sea-sea and sea-valence couplings to the meson dressings [25]. The square of the sea-sea quark charge ensures one-loop sea-sea photon coupling contributions are all positive, whereas the sea-valence contributions depend on the charge of the meson. Charged mesons contribute positively, and neutral mesons (having opposite charged quarks) contribute negatively. These sea-quark loop contributions have been examined in finite-range regularized chiral effective field theory [26], which enables one to model the significance of these changes to the nonanalytic terms of the expansion. The net correction is positive but small relative to the polarizabilities reported herein, and we refer the interested reader to Ref. [26] for further details.

We also performed an initial calculation using quenched gauge configurations. These were $32^3 \times 40$ lattices using a FLIC fermion action and Symanzik improved gauge action at $\beta = 4.52$. There were 192 configurations at seven quark masses, corresponding to $m_\pi = 0.8400$, 0.7745, 0.6929, 0.6261, 0.5399, 0.4353, 0.2751 GeV. The lattice spacing was $a = 0.128$ fm, and like the dynamical calculation, boundary conditions were periodic for the spatial dimensions and fixed for the time boundary. Values for $m_\pi L$ range from 17.4 to 5.7. We used fields corresponding to $n = 1$, -2, 4, -8 in the quantization condition to save on computation.

IV. MAGNETIC MOMENT

A. Formalism

When a charge or system of charges with angular momentum is placed in an external magnetic field, it is energetically favorable to have its axis either aligned or antialigned with the direction of the field. The tendency of the system to align with the field is proportional to the magnetic moment of the system and the strength of the field.

We calculate zero-momentum projected correlation functions containing spin-up and spin-down components in the (1, 1) and (2, 2) positions of the Dirac matrix, respectively. Here we are using the Pauli representation for the gamma matrices. For a magnetic field aligned to the axis of the spin, we see the magnetic moment manifest as a shift in the energy which has the same magnitude, but opposite sign, for spin up and spin down.

We make use of the sign difference in the energy shift between spin up and spin down in order to isolate the magnetic moment term from the expansion of the energy. Taking the difference of the spins,

$$\delta E(B) = \frac{1}{2}(E_\uparrow(B) - E_\downarrow(B)) = -\mu B. \tag{11}$$

In addition to the bare mass and polarizability term, this difference also cancels out the Landau energy term $e|B|/2M_N$. For the neutron, one expects this term to be zero because it is proportional to the charge. However, for the proton, even though taking the difference cancels out the term, it can still affect the results. This is because we use a standard projection to zero momentum in our correlation functions, but when Landau levels are present, one obtains a superposition of Landau states. As we are working within a particular choice of gauge for the magnetic field, the strengths of the superpositions are dependent on this choice of gauge. There are proposed techniques for dealing with the Landau levels [16], but we have found that the effect on the magnetic moment results is small, and defer this issue to a subsequent investigation.

In terms of correlation functions, there are multiple valid ways of taking the spin difference—for example, fitting the energy and then taking the difference, or combining correlation functions and then fitting. By taking a combination of correlation functions before fitting for the energy, the statistical error is greatly reduced and provides strong constraints on the fit regime. This is because the errors are highly correlated between the zero and nonzero field correlation functions, meaning the fluctuations do not change significantly due to the field. The combination required for isolating the moment term can be written as

$$\delta E(B,t) = \frac{1}{2}\left(\ln\left(\frac{G_\uparrow(B,t)}{G_\uparrow(0,t)}\frac{G_\downarrow(0,t)}{G_\downarrow(B,t)}\right)\right)_{\text{fit}}. \tag{12}$$

The inclusion of the bare correlation functions without a magnetic field in this expression is not strictly necessary, but it is useful in correcting for the small statistical difference between spin-up and spin-down zero-field energies and making the zero-field point zero by construction. We also define spin up to mean aligned with the magnetic field and spin down to mean antialigned to the field, so that we can treat all the fields as positive in our discussion.

B. Results

Figure 1 shows the energy shift from the difference of spin-up and spin-down nucleons for the heaviest quark mass at all four nonzero magnetic field strengths. Both the proton and the neutron show a good linear progression over the field strengths as expected, with excellent plateaus.

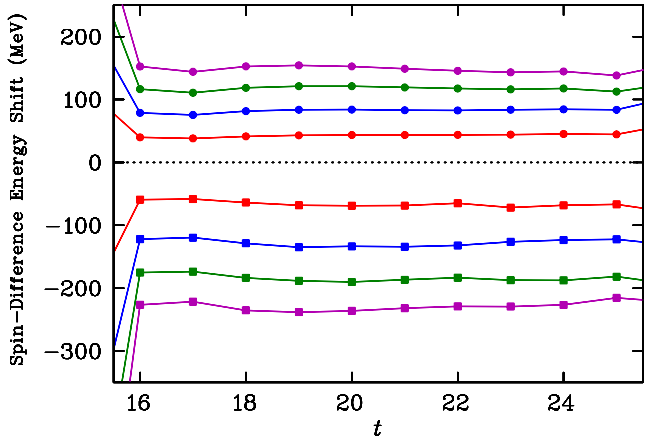

FIG. 1 (color online). Spin-difference energy shift of Eq. (12) for the heaviest quark mass at all four field strengths. The proton values are given by the squares and the neutron values by the circles. The shifts increase in magnitude with the strength of the field.

There is very little excited-state contribution to the energy shifts in evidence. The neutron effective energy is generally slightly smoother than that of the proton, with similar results for the other quark masses. The larger errors in the proton energies may be due to the effect of the Landau levels in the momentum projection. At the two higher field strengths, there tends to be a small drift in the value over time, with the true plateau perhaps only occurring at around time slice 23 or 24. This leads to a slight difference in the value of the energy shift depending on the choice of fit window; however, this has little effect on the magnetic moment result for reasons described below.

Figures 2 and 3 show the spin-difference energy shifts plotted against the magnetic field strength. These are fit to a linear coefficient which gives the magnetic moment. In order to fit the largest field strength, and to a lesser extent the second largest, we had to include a cubic term in the fit. With the cubic term included, all four data points are fit easily. However, the first two points are the main drivers of the linear coefficient, and therefore the magnetic moment value.

The cubic term is able to absorb some variation in the energy shifts at the higher field strengths, which is why the drift in the effective energy shown in Fig. 1 does not significantly affect the resulting magnetic moment value. This is seen in Table I, which gives values of the neutron magnetic moment for a number of fit windows. The same window is used at every field strength in order to maintain consistency and prevent introducing systematic errors. Only changes in the field strength act to change the measured energy. The values agree well within errors for all but the earliest fit window, suggesting that time slice 19 is slightly too early to fit due to excited state contamination. Large χ^2/d.o.f. values also exclude this fit window.

In considering other quark masses, we consistently select fit window 20–22 to provide the same fit window for every field strength and quark mass. Again, only changes in the field strength and quark mass act to change the energy.

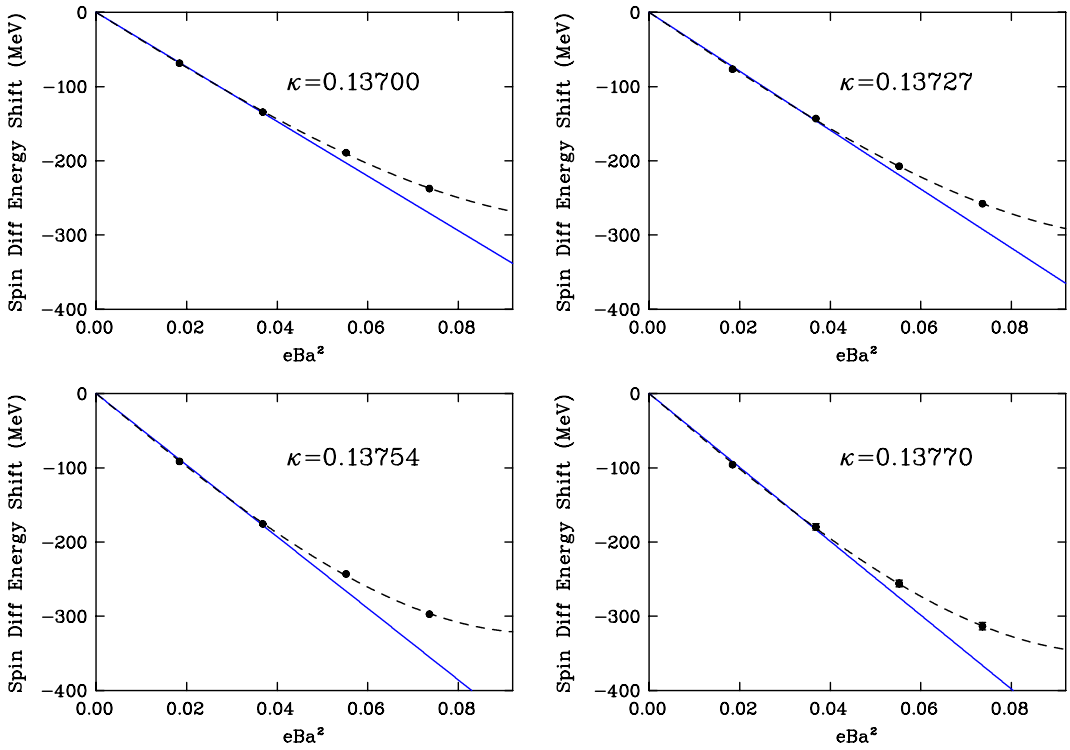

FIG. 2 (color online). Fits of the spin-difference energy shift to the field strength at each quark mass for the proton. The solid line is a purely linear fit to just the first two points, and the dashed line is a linear-plus-cubic fit to all four points.

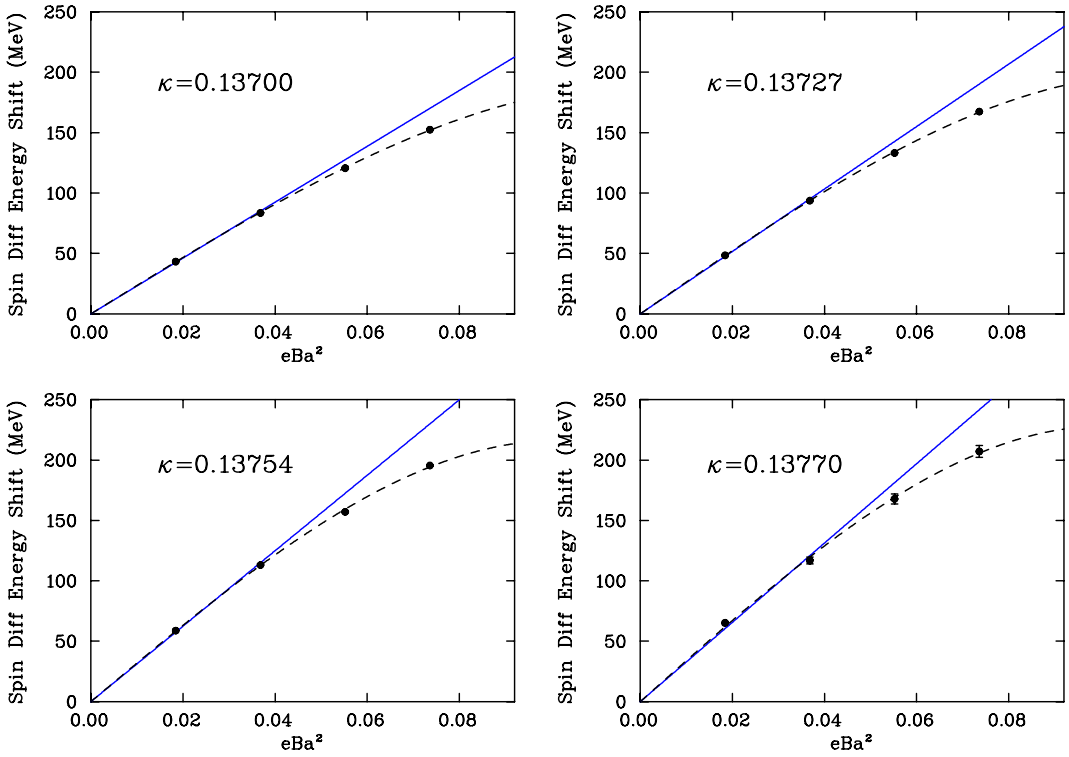

FIG. 3 (color online). Fits of the spin-difference energy shift to the field strength at each quark mass for the neutron. The solid line is a purely linear fit to just the first two points, and the dashed line is a linear-plus-cubic fit to all four points.

A consistent set of larger fit windows was considered, and good agreement between the magnetic moment values was observed for most fit windows. However, many of these fits produced unacceptably large χ^2/d.o.f. values, and we take the more conservative and consistent fit window to avoid introducing a systematic error.

Given that the first two points are the main drivers of the magnetic moment, we performed a purely linear fit to the first two points. We find the the linear coefficients determined from both two- and four-point fits agree well within errors. Since the fit is naturally constrained to go through zero, two nonzero field points are sufficient. Moreover, our field strengths are small enough to ensure the higher-order contributions are negligible at these two points.

The magnetic moment is reported in units of nuclear magnetons via

$$\mu = -\frac{\delta E}{eB}\left[\frac{e}{2M_N}\right]2M_N, \tag{13}$$

where we have started with Eq. (11) and introduced the elementary charge e since we actually fit the energy shift against eB, then bring in twice the physical nucleon mass M_N in order to get the nuclear magneton ($\mu_N = \frac{e\hbar}{2M_N}$), given that we are using natural units ($c = \hbar = 1$).

Figures 4 and 5 show the proton and neutron magnetic moment results, compared with a three-point function calculation for reference [27]. Although the finite-volume effects in a three-point function computation are not the same as those in our background field calculation, the results compare favorably. The lines are chiral fits to the dynamical results using the simple model of Ref. [28] and guide the anticipated trajectory to the physical point. The reason the extrapolated values are smaller in magnitude than the experimental values is understood to be due to finite volume effects [29], as those have not been examined herein.

TABLE I. Magnetic moment values for the neutron at each κ value for a variety of fit windows.

Window	0.13700	0.13727	0.13754	0.13770
19–21	−1.187(12)	−1.300(13)	−1.420(16)	−1.486(36)
20–22	−1.194(11)	−1.317(15)	−1.462(22)	−1.483(30)
21–23	−1.198(13)	−1.338(20)	−1.454(27)	−1.500(40)
22–24	−1.201(15)	−1.343(25)	−1.454(32)	−1.508(49)
20–24	−1.199(10)	−1.321(15)	−1.462(20)	−1.485(31)

V. MAGNETIC POLARIZABILITY

A. Formalism

The magnetic polarizability is a measure of the deformation of a nonpointlike particle when it is placed in a magnetic field. This deformation causes a change in the energy which we can measure using the background field method. The effect of the magnetic polarizability is second

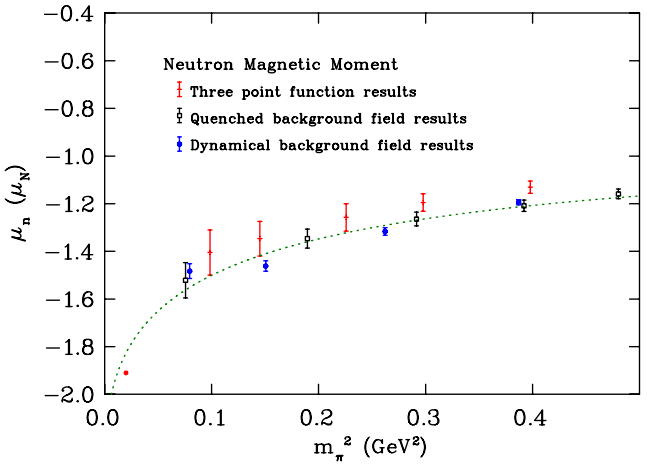

FIG. 4 (color online). Neutron magnetic moment as a function of pion mass squared. The leftmost point gives the experimental value [30]. The dashed line is a chiral extrapolation of the dynamical points.

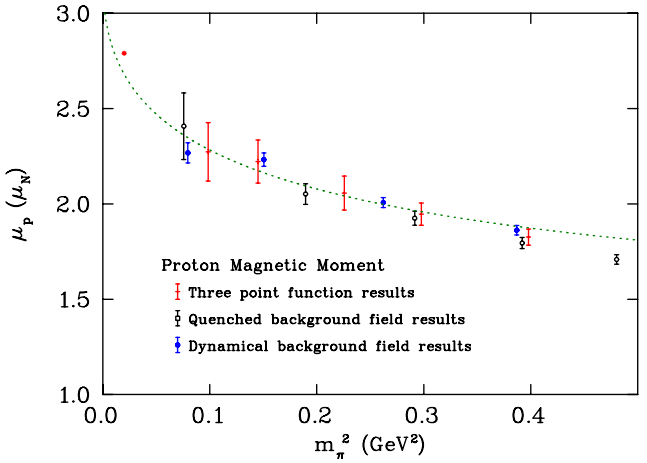

FIG. 5 (color online). Proton magnetic moment as a function of pion mass squared. The leftmost point gives the experimental value [30]. The dashed line is a chiral extrapolation of the dynamical points.

order in B. This means that at the "small" field strengths we are using, the effect is much smaller than that due to the magnetic moment, which can make it hard to measure.

To extract the polarizability from the energy, we take the average of spin-up and spin-down energy shifts to remove the magnetic moment term and explicitly subtract the zero-field mass. The spin-averaged energy shift is

$$\delta E_\beta(B) = \frac{1}{2}((E_\uparrow(B) - E_\uparrow(0)) + (E_\downarrow(B) - E_\downarrow(0))) = \frac{e|B|}{2M_N} - \frac{4\pi}{2}\beta B^2.$$

This leaves us with the polarizability term, but also with another term due to the Landau energy. This energy arises from the quantization of orbits for charged particles in magnetic fields and cannot be isolated from the relevant polarizability term. As a result, it is difficult to calculate magnetic polarizabilities of charged particles, because there is not only the ground-state Landau energy but also a tower of Landau levels with energy $(2n+1)\frac{e|B|}{2M_N}$. The need for small field strengths makes the Landau-level problem even worse, because it means the Landau levels are closer together, which makes it take longer in Euclidean time for the levels above the ground state to be exponentially suppressed [16].

The influence of the Landau levels on the proton is readily apparent in Fig. 6, which shows the spin average of the energy shift due to the field. Since the experimental value of the magnetic polarizability is approximately the same for the proton and neutron, we would expect this to look similar to the neutron results in Fig. 7. Instead, we see much larger errors and no consistent trend across the field strengths. Due to the large and unpredictable systematic errors caused by this effect, we are not presenting values for the magnetic polarizability of the proton in this first exploratory investigation. For an elementary particle with zero charge, there is no Landau effect. However, the neutron is an extended object, and the u and d quarks are not distributed symmetrically. This admits the possibility of nontrivial Landau-level effects. While one might anticipate these effects are small, evidence below reveals an important contribution.

As with the magnetic moment, we construct ratios of correlation functions, which we then fit for an effective energy,

$$\delta E_\beta(B,t) = \frac{1}{2}\left(\ln\left(\frac{G_\uparrow(B,t)}{G_\uparrow(0,t)}\frac{G_\downarrow(B,t)}{G_\downarrow(0,t)}\right)\right)_{\text{fit}}. \quad (14)$$

In this case, the zero-field correlators are necessary to remove the bare neutron mass. Combining the correlation functions

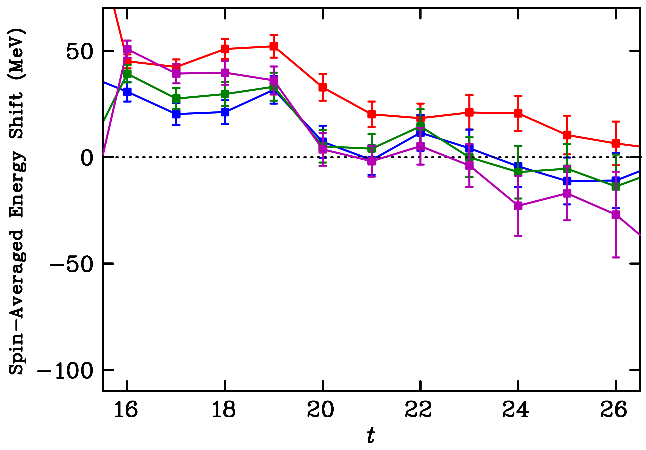

FIG. 6 (color online). Proton spin-averaged energy shift for the heaviest quark mass at all field strengths. The top line is the smallest field strength, with the other three agreeing well within errors for most of the relevant time frame.

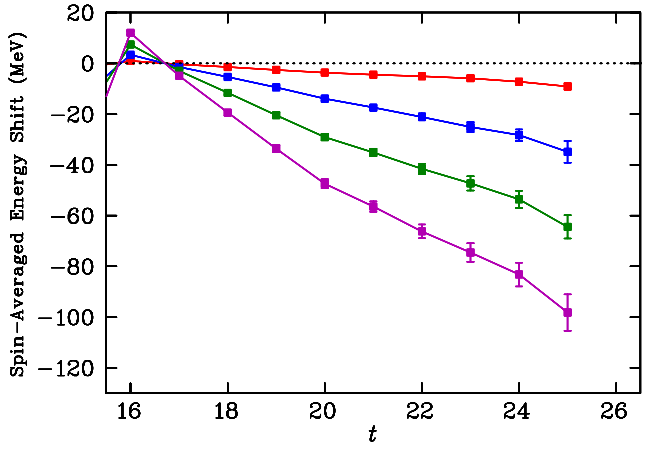

FIG. 7 (color online). Neutron spin-averaged energy shift for the heaviest quark mass at all four field strengths. The magnitude of the shift increases with the field strength.

before fitting is especially important in the polarizability case, because the energy shift is smaller than the errors on the zero-field mass. This means that if the correlated errors were not allowed to cancel before the fit, we would not see a clear signal for the shift due to the polarizability.

B. Results

Figure 7 gives the spin-averaged effective energy shift for the heaviest quark mass considered. Unlike the spin-difference case, the plateau behavior is quite poor, with a fairly constant downward slope that begins to plateau only after significant noise is appearing. Only in the case of the smallest field strength does something like a real plateau appear before the signal is lost to noise. The situation is very similar at other quark masses, with the errors getting larger and the noise coming earlier at lighter quark masses, as seen in Fig. 8 for the lightest quark mass considered. The plots show that at each field strength, the energy shift starts at approximately zero and grows with Euclidean time. Typically the lack of a plateau in an effective energy plot is due to the presence of excited state energies in addition to the ground state. Figure 9, illustrating the bare effective mass, does reveal a systematic drift in the energy, suggesting some improvement in the interpolating field may be possible.

In order to check for excited-state overlap and try to improve the plateau behavior, we looked at different sources. We experimented with a number of different source smearings, trying 16 and 35 sweeps in addition to our usual 100. We also tried a point source on the basis that it should have no bias towards any shape and may therefore reach the required form more quickly. Figure 10 shows the energy shift due to the field for all smearing choices at the heaviest quark mass and the smallest field. The three smeared sources have different behavior but agree well within errors by time slice 24, just before the signal is lost to noise. The point source has large excited-state contributions and approaches agreement with the other sources as the signal is lost.

We notice from these plots that the best plateau behavior comes from 16 sweeps of smearing for spin up and 100 sweeps of smearing for spin down. To take advantage of this, we constructed a spin average from the spin-up correlation function with 16 sweeps and the spin-down correlation function with 100 sweeps. We found the improved plateau behavior shown in Fig. 11, leading us to investigate further the possibility of combining different source smearings.

The variational method as implemented in Ref. [31] involves using an $n \times n$ correlation matrix $G_{ij}(t)$ constructed from different source and sink smearing levels to solve a pair of eigenvalue equations. The right and left eigenvectors u_j^α and v_i^α can then be used to project out

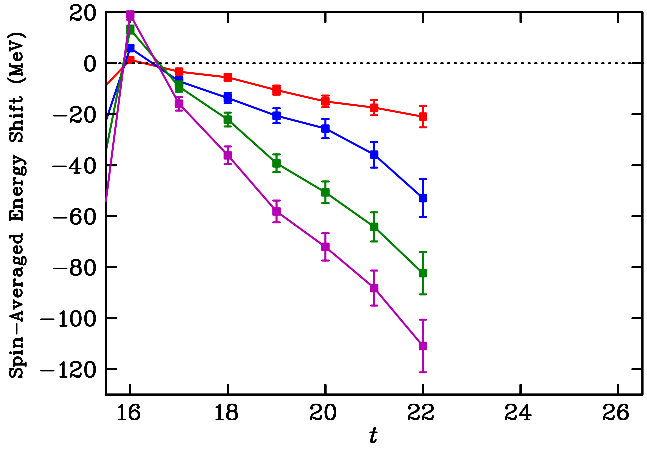

FIG. 8 (color online). Neutron spin-averaged energy shift for the lightest quark mass at all four field strengths. The magnitude of the shift increases with the field strength.

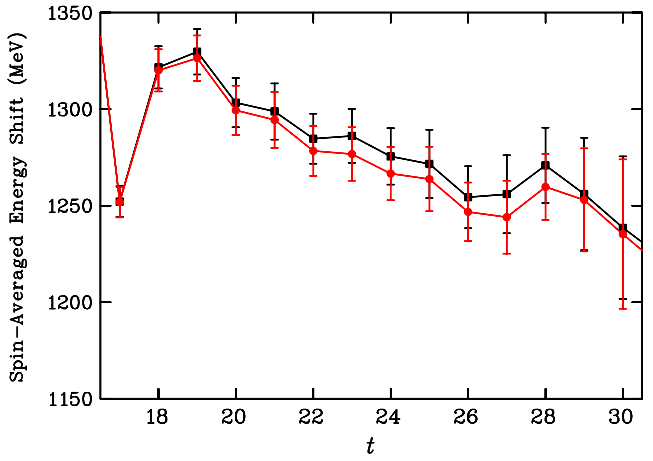

FIG. 9 (color online). Spin-averaged effective mass for the neutron at $\kappa = 0.13727$. The top line (squares) is for zero magnetic field, and the bottom line (circles) is with the smallest field strength considered.

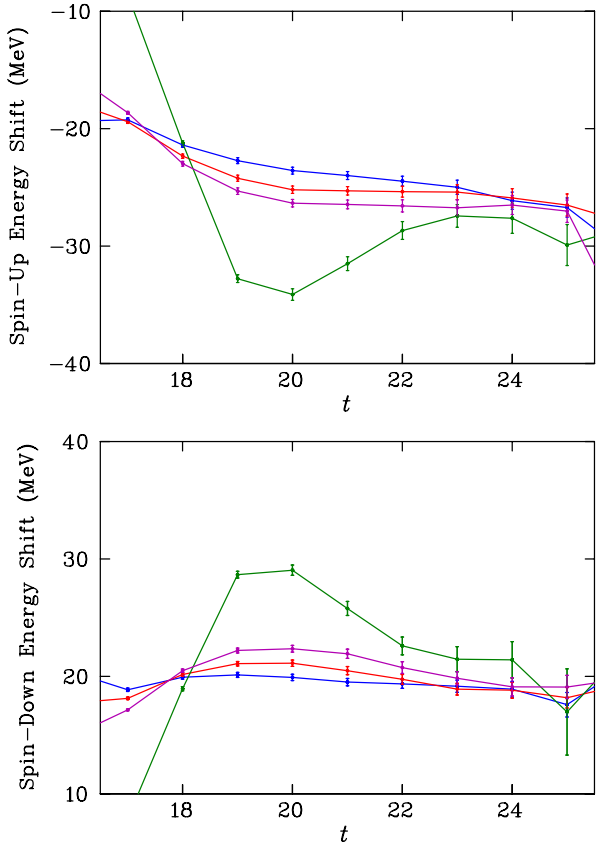

FIG. 10 (color online). Energy shift at the smallest field strength. For spin up, we have from top to bottom 100, 35, 16 sweeps of smearing and point source; for spin down, the order is reversed.

energy eigenstates α to effectively isolate the $n-1$ lowest energy states,

$$G^{\alpha}(t) = v_i^{\alpha} G_{ij}(t) u_j^{\alpha}. \tag{15}$$

Combining correlation matrix techniques with the background field method introduces new considerations. Normally, the eigenvector analysis is performed on spin-averaged correlation functions because spin up and spin down are equal up to statistics. For a background field calculation, we need to consider spin up and spin down separately, with each field strength getting its own eigenvector equation to solve. This is necessary, as each field and spin combination has a separate Hilbert space of energy eigenstates. In other words, the eigenvectors u_i^{α} and v_j^{β} are field and spin dependent, and a recurrence relation leading to a generalized eigenvalue equation cannot be written for combinations of spins and fields. After solving the eigenvalue equations, we construct the same ratio as in Eq. (14), but using the projected correlation functions from Eq. (15).

We first performed a variational analysis using a 2×2 correlation matrix made from 16 and 100 sweeps of smearing. The resultant spin-average energy shift using the ground-state projected correlation functions was approximately equal to the original 16- and 100-sweep correlation

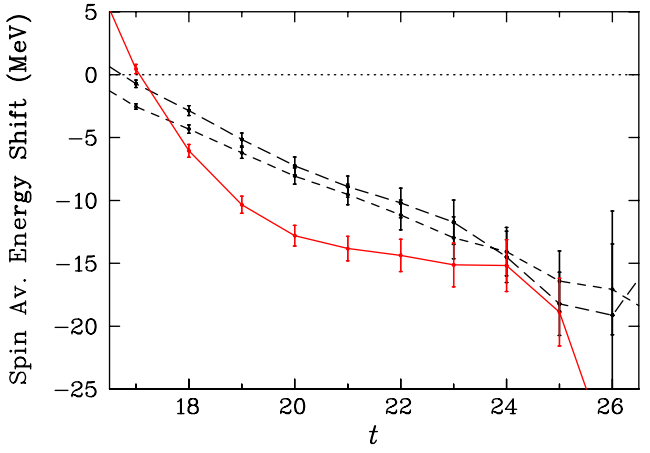

FIG. 11 (color online). Spin-averaged effective energy shift for the heaviest quark mass at the smallest background field. The dashed lines are for 16 and 100 sweeps of smearing, and the solid line is from the combination of spin up with 16 sweeps and spin down with 100 sweeps.

functions. The plateau behavior was not noticeably better than using either of the smearings alone. We also tried other various combinations of sources with different smearings including 16, 35 and 100 sweeps, as well as different interpolating fields in 3×3 and 4×4 correlation matrices. None of these combinations was found to result in a statistically significant improvement in the plateau behavior.

The conclusion that must be drawn from this is that the neutron is not free from Landau-level effects. As highlighted earlier, the neutron is an extended object having an asymmetry in the distribution of the u and d quark flavors. This asymmetry gives rise to a nontrivial charge radius for the neutron. Thus one must expect that the individual quark sectors will respond to the background field and have an associated Landau-level response.

Even if the neutron had a perfect symmetry between u and d quark distributions, the different electric charges of the quarks would enable the external field interactions to break this symmetry. Thus, even a perfectly symmetric distribution of u and d quarks in QCD would admit a Landau-level response at the quark level due to QED effects.

One can imagine a case where QCD is so strong, the symmetry breaking induced by the field is negligible. However, this is not the case. The u-d symmetry is broken by QCD itself. This gives rise to a nontrivial neutron charge radius and exposes regions of nontrivial charge density that can respond to the background field. The relatively small effective charge gives rise to a very closely spaced set of Landau levels which decays smoothly in the manner we observe.

Fortunately, our consideration of several different fermion source smearings has provided some indication of the onset of ground-state dominance. Referring to Fig. 10, agreement in the energy shift for all smeared sources considered is observed at $t = 24$. Different fermion source

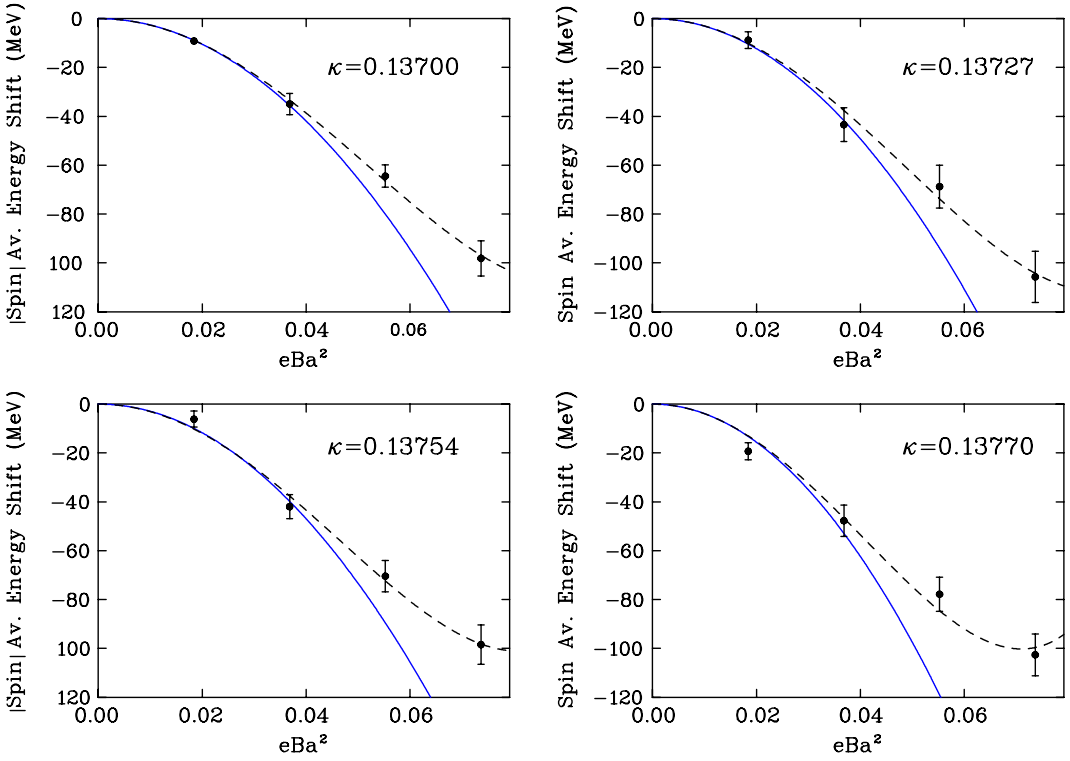

FIG. 12 (color online). The spin-averaged energy shifts as a function of the background field strength for the neutron. The solid line is a pure quadratic fit to the first two points, while the dashed line is a fit of all the points to a quadratic plus quartic.

smearings give rise to different superpositions of excited states. Because all the different superpositions of states agree at this point, we are confident the excited states have been suppressed relative to the ground state. In proceeding, we take a very cautious and conservative approach by determining the energy shifts from the last time slice available prior to the onset of significant noise. While the uncertainties are perhaps somewhat larger than desired, we prefer to report a correct answer with a large uncertainty as opposed to a speculative result with an underestimated error bar.

Figure 12 shows fits of these spin-averaged energy shifts as a function of the field strength. In addition to the quadratic polarizability term, we required a quartic term in order to fit the higher field strengths. This higher-order term is small at the heaviest mass but starts to become significant at the lighter masses.

Figure 13 shows our neutron magnetic polarizability results with a comparison between our quenched and dynamical calculations. The quenched and dynamical results agree well within errors. The dashed line shows a fit of the dynamical results to

$$\beta = a + \frac{b}{m_\pi} + c\ln(m_\pi) + dm_\pi^2,$$

where the values of coefficients b and c were set from values calculated in χPT [32], and a and d are fit freely. Although this formula does not account for the vanishing sea-quark charges and the finite volume of the lattice simulations, it does provide a reasonable forum for the first comparison of lattice QCD results and experiment. The extrapolated value of $1.8 \pm 0.2 \times 10^{-4}$ fm^3 is well within the error bar of the experimental value.

A more rigorous chiral extrapolation of our results in partially quenched QCD accounting for the finite volume of the lattice and the neutral electric charges of the sea quarks

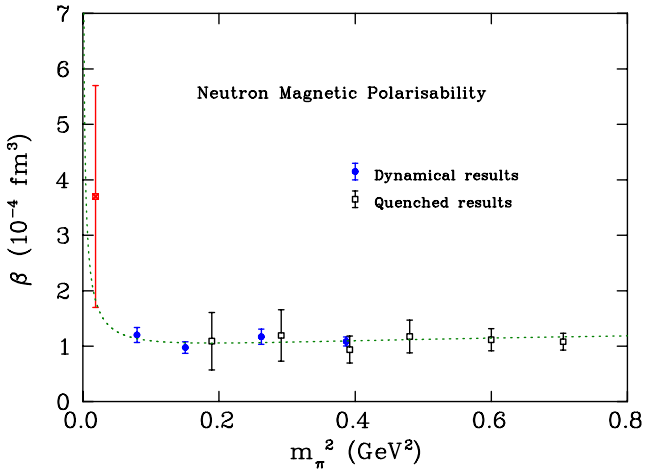

FIG. 13 (color online). Neutron magnetic polarizability as a function of pion mass. The red point illustrates the experimental value [30]. The line represents a fit of χPT to the dynamical fermion lattice results.

TABLE II. Summary of the main results.

κ	m_π (MeV)	a (fm)	μ_n (μ_N)	μ_p (μ_N)	β_n (10^{-4} fm^3)
0.13700	702	0.1022(15)	−1.19(1)	1.86(3)	1.08(8)
0.13727	572	0.1009(15)	−1.32(2)	2.01(3)	1.17(14)
0.13754	413	0.0961(13)	−1.46(2)	2.23(4)	0.98(10)
0.13770	293	0.0951(13)	−1.48(3)	2.27(5)	1.20(13)

has been carried out by Hall *et al.* in Ref. [26]. There, the volume dependence of the polarizability is examined to provide a guide to future lattice QCD investigations. With an improved calculation at near physical pion mass on a large lattice volume exceeding 5 fm on a side [26], we anticipate a lattice result that verifies the significant chiral curvature generated by the partially quenched finite-volume pion cloud.

Moreover, the contributions of the dynamical sea-quark degrees of freedom are modeled in Ref. [26] to provide a comprehensive comparison with experiment. The final value for the magnetic polarizability of the neutron in infinite-volume full QCD is $1.93 \pm 0.11 \pm 0.11 \times 10^{-4}$ fm^3 with systematic and statistical uncertainties indicated.

VI. CONCLUSION

We have performed the first calculations of the magnetic moment and magnetic polarizability of the neutron in a uniform background field. Results for the magnetic moment are very clear and agree well with previous calculations. The approach can be used in a precision manner to directly determine the magnetic moment without the need for extrapolating form factors in Q^2.

Magnetic polarizability calculations have proved more difficult due to late-appearing plateaus. Consideration of a variety of fermion source smearings and the agreement observed at the largest Euclidean times available herein provide an indication of ground-state saturation, enabling a determination of the magnetic polarizability of the neutron. We have calculated dynamical fermion results that agree with our previous quenched results and have a promising approach to the experimental value. A summary of the numerical results is given in Table II.

An important discovery is a nontrivial role for Landau levels in neutron correlation functions. While the neutron's zero (total) charge was thought to render such contributions negligible, the asymmetric distribution of charge within the neutron admits nontrivial contributions from each of the quark sectors.

Studies in chiral effective field theory and in lattice QCD are needed to further explore finite-volume effects and the subtle role of dynamical fermion sea-quark loops. It is also important to develop new fermion sources/sinks that can respond to the effects of the Landau energy at the individual quark-sector level, enabling better isolation of the ground-state energy shift.

ACKNOWLEDGMENTS

We are grateful for the generosity of the PACS-CS Collaboration for providing the gauge configurations used in this study. The contributions of the ILDG in making the configurations accessible is also appreciated. This research was undertaken with the assistance of resources at the NCI National Facility in Canberra, Australia, and the iVEC facilities at the University of Western Australia. These resources were provided through the National Computational Merit Allocation Scheme, supported by the Australian Government. We also acknowledge the contributions of eResearch SA in maintaining our supercomputers. This research is supported by the Australian Research Council.

[1] G. Martinelli and C. T. Sachrajda, Nucl. Phys. **B316**, 355 (1989).
[2] T. Draper, R. M. Woloshyn, and K.-F. Liu, Phys. Lett. B **234**, 121 (1990).
[3] D. B. Leinweber, R. M. Woloshyn, and T. Draper, Phys. Rev. D **43**, 1659 (1991).
[4] C. W. Bernard, T. Draper, K. Olynyk, and M. Rushton, Phys. Rev. Lett. **49**, 1076 (1982).
[5] G. Martinelli, G. Parisi, R. Petronzio, and F. Rapuano, Phys. Lett. **116B**, 434 (1982).
[6] J. Smit and J. C. Vink, Nucl. Phys. **B286**, 485 (1987).
[7] H. Rubinstein, S. Solomon, and T. Wittlich, Nucl. Phys. **B457**, 577 (1995).
[8] M. Burkardt, D. B. Leinweber, and X.-m. Jin, Phys. Lett. B **385**, 52 (1996).
[9] L. Zhou, F. X. Lee, W. Wilcox, and J. C. Christensen, Nucl. Phys. B, Proc. Suppl. **119**, 272 (2003).
[10] F. X. Lee, R. Kelly, L. Zhou, and W. Wilcox, Phys. Lett. B **627**, 71 (2005).
[11] F. Lee, L.-M. Zhou, W. Wilcox, and J. Christensen, *Proc. Sci.*, LAT2005 (**2006**) 031.
[12] F. X. Lee, S. Moerschbacher, and W. Wilcox, Phys. Rev. D **78**, 094502 (2008).
[13] C. Aubin, K. Orginos, V. Pascalutsa, and M. Vanderhaeghen, Phys. Rev. D **79**, 051502 (2009).
[14] W. Detmold, B. Tiburzi, and A. Walker-Loud, Phys. Rev. D **81**, 054502 (2010).

[15] H. R. Fiebig, W. Wilcox, and R. M. Woloshyn, Nucl. Phys. **B324**, 47 (1989).
[16] B. Tiburzi and S. Vayl, Phys. Rev. D **87**, 054507 (2013).
[17] S. Aoki *et al.* (PACS-CS Collaboration), Phys. Rev. D **79**, 034503 (2009).
[18] M. G. Beckett, P. Coddington, B. Joó, C. M. Maynard, D. Pleiter, O. Tatebe, and T. Yoshie, Comput. Phys. Commun. **182**, 1208 (2011).
[19] W. Freeman, A. Alexandru, F. Lee, and M. Lujan, *Proc. Sci.*, LATTICE2012 (**2012**) 015.
[20] D. B. Leinweber, Phys. Rev. D **53**, 5115 (1996).
[21] D. B. Leinweber, Phys. Rev. D **69**, 014005 (2004).
[22] D. Leinweber, S. Boinepalli, I. Cloet, A. Thomas, A. Williams, R. Young, J. Zanotti, and J. Zhang, Phys. Rev. Lett. **94**, 212001 (2005).
[23] R. Lewis, W. Wilcox, and R. Woloshyn, Phys. Rev. D **67**, 013003 (2003).
[24] T. Doi, M. Deka, S.-J. Dong, T. Draper, K.-F. Liu, D. Mankame, N. Mathur, and T. Streuer, Phys. Rev. D **80**, 094503 (2009).
[25] W. Detmold, B. Tiburzi, and A. Walker-Loud, Phys. Rev. D **73**, 114505 (2006).
[26] J. Hall, D. Leinweber, and R. Young, arXiv:1312.5781.
[27] S. Boinepalli, D. B. Leinweber, A. G. Williams, J. M. Zanotti, and J. B. Zhang, Phys. Rev. D **74**, 093005 (2006).
[28] D. B. Leinweber and A. W. Thomas, Phys. Rev. D **62**, 074505 (2000).
[29] J. M. M. Hall, D. B. Leinweber, and R. D. Young, Phys. Rev. D **85**, 094502 (2012).
[30] J. Beringer *et al.* (Particle Data Group), Phys. Rev. D **86**, 010001 (2012).
[31] M. S. Mahbub, W. Kamleh, D. B. Leinweber, P. J. Moran, and A. G. Williams, AIP Conf. Proc. **1432**, 261 (2012).
[32] V. Bernard, N. Kaiser, U. G. Meissner, and A. Schmidt, Z. Phys. A **348**, 317 (1994).